



## ORIGINAL ARTICLE

# Association of anaplastic lymphoma kinase variants and alterations with ensartinib response duration in non-small cell lung cancer

Donghui Hou<sup>1</sup>  | Xiaomin Zheng<sup>2</sup> | Wei Song<sup>3</sup> | Xiaoqing Liu<sup>4</sup> | Sicong Wang<sup>5</sup> | Lina Zhou<sup>1</sup> | Xiuli Tao<sup>6</sup> | Lv Lv<sup>6</sup> | Qi Sun<sup>7</sup> | Yujing Jin<sup>6</sup> | Zewei Zhang<sup>6</sup> | Lieming Ding<sup>8</sup> | Ning Wu<sup>1,6</sup> | Shijun Zhao<sup>1</sup> 

<sup>1</sup>Department of Diagnostic Radiology, National Cancer Center/National Clinical Research Center for Cancer/Cancer Hospital, Chinese Academy of Medical Sciences and Peking Union Medical College, Beijing, China

<sup>2</sup>Department of Endocrinology, Chui Yang Liu Hospital affiliated to Tsinghua University, Beijing, China

<sup>3</sup>Department of Radiology, Peking Union Medical College Hospital, Chinese Academy of Medical Sciences, Peking Union Medical College, Beijing, China

<sup>4</sup>Department of Pulmonary Oncology, The Fifth Medical Centre, Chinese PLA General Hospital, Beijing, China

<sup>5</sup>GE Healthcare, Life Sciences, Beijing, China

<sup>6</sup>PET-CT Center, National Cancer Center/National Clinical Research Center for Cancer/Cancer Hospital, Chinese Academy of Medical Sciences and Peking Union Medical College, Beijing, China

<sup>7</sup>Department of Radiology, Harbin Medical University Cancer Hospital, Harbin, China

<sup>8</sup>Betta Pharmaceuticals Co., Ltd., Hangzhou, China

## Correspondence

Shijun Zhao, Department of Diagnostic Radiology, National Cancer Center/National Clinical Research Center for Cancer/Cancer Hospital, Chinese Academy of Medical Sciences and Peking Union Medical College, No. 17, Panjiayuan Nanli, Beijing, 10021, China.  
Email: zsj.2001@163.com

Ning Wu, Department of Diagnostic Radiology and PET-CT Center, National Cancer Center/National Clinical Research Center for Cancer/Cancer Hospital, Chinese Academy of Medical Sciences and Peking Union Medical College, No. 17, Panjiayuan Nanli, Beijing, 10021, China.  
Email: cjr.wuning@vip.163.com

## Funding information

Beijing Municipal Science and Technology Project, Grant/Award Number: Z201100005620002; CAMS Innovation Fund for Medical Sciences, Grant/Award Number: Grant/Award Number: 2019-I2M-2-002, 2017-I2M-1-005; National Key R&D Program of China: 2017YFC1308700; National Natural Science Foundation of China, Grant/Award Number: 81771830

## Abstract

**Background:** Here, we aimed to assess the association of ALK variants and alterations with ensartinib response duration in NSCLC, and explore the potential value of computed tomography (CT) radiomic features in predicting progression-free survival (PFS).

**Methods:** We enrolled 88 patients with identified ALK variant NSCLC in a multicenter phase 2 trial, and assessed the impact of ALK variants and secondary ALK alterations on the clinical outcome (response duration) of patients receiving ensartinib. We also established a multifactorial model of clinicopathological and quantitative CT radiomic features to predict PFS and risk stratification. Kaplan–Meier analysis was conducted to identify risk factors for tumor progression.

**Results:** Univariate analysis indicated a statistical difference ( $p = 0.035$ ) in PFS among ALK variants in three classifications (V1, V3, and other variants). Secondary ALK alterations were adversely associated with PFS both in univariate ( $p = 0.008$ ) and multivariate ( $p = 0.04$ ) analyses and could identify patients at high risk for early progression in the Kaplan–Meier analysis ( $p = 0.002$ ). Additionally, response duration to crizotinib <1 year and liver metastasis were adversely associated with PFS. The combined model, composed of clinicopathological signature and CT radiomic signature, showed good prediction ability with the area under the receiver operating characteristic curve being 0.85, and 0.89 in the training and validation dataset respectively.

**Conclusions:** Our study showed that secondary ALK alterations were adversely associated with ensartinib efficacy, and that ALK variants might not correlate with PFS.

The quantitative radiomic signature provided added prognostic prediction value to the clinicopathological features.

#### KEYWORDS

ALK fusion, ensartinib, gene mutation, progression-free survival, radiomics

## INTRODUCTION

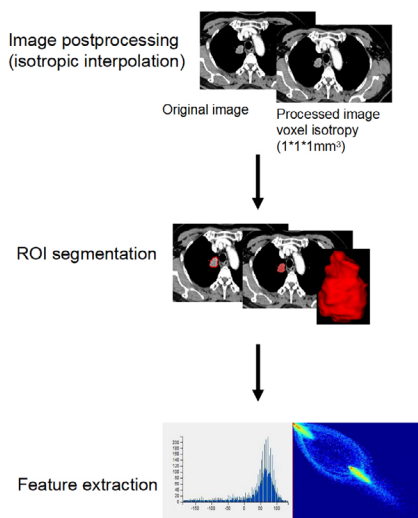
Anaplastic lymphoma kinase (ALK) gene fusion occurs in approximately 3%–7% of patients with non-small cell lung cancer (NSCLC) and is sensitive to ALK tyrosine kinase inhibitors (TKIs).<sup>1</sup> There are various ALK gene fusion partners, including predominant partner echinoderm microtubule-associated protein-like 4 (EML4)<sup>2</sup> and other rare non-EML4 partners, such as HIP1,<sup>3</sup> KLC1,<sup>4</sup> KIF5B,<sup>5</sup> TPR,<sup>6</sup> and TFG.<sup>7</sup> More than 15 EML4-ALK variants have been identified based on the occurrence of EML4 internal breakpoints at different sites; of these, variant 1 (v1; exon 13 of EML4 fused to exon 20 of ALK [E13;A20]), and variant 3a/b (exon 6a/b of EML4 fused to exon 20 of ALK [E6a/b;A20]) are the most frequent.<sup>2</sup>

Since the approval of first-generation ALK inhibitor, crizotinib, multiple second- (e.g., ensartinib, alectinib, and brigatinib) and third-generation (e.g., lorlatinib) ALK-TKIs have been approved for the treatment of patients with ALK-rearranged NSCLC, all with higher potency or greater central nervous system penetration than crizotinib.<sup>8–12</sup> Although these ALK inhibitors have significantly improved clinical efficacy, the clinical outcomes vary widely among patients.

Studies have found that ALK fusion variants might affect the therapeutic efficacy of ALK inhibition, but these results are controversial.<sup>13–18</sup> Most studies have suggested that EML4-ALK fusion V3 is a high-risk feature conferring early ALK-TKI treatment failure and worse overall survival,<sup>13–15</sup> whereas several other studies have found that V3 is associated with significantly longer progression-free survival (PFS) than V1 in patients with NSCLC treated with lorlatinib.<sup>16</sup> Moreover, another study suggested that ALK variants might not be correlated with the clinical response to crizotinib.<sup>17,18</sup> Therefore, it is necessary to further investigate how ALK variants may affect the efficacy of ALK-TKIs.

Although tissue biopsy is considered the standard procedure for defining the molecular status of various solid tumors, including NSCLC, it has several limitations, including procedural invasiveness and the risk of false-negative results due to tumor heterogeneity or low tumor cellularity. The circulating tumor DNA (ctDNA) test is an important complement to tissue biopsies, providing a means to predict treatment response and monitoring resistance in patients with NSCLC receiving targeted therapies; however, because circulating cell-free tumor-derived DNA is diluted with normal DNA, ctDNA analysis is technically challenging, requiring both high sensitivity and accuracy. It

#### Radiomic workflow



#### Study flowchart

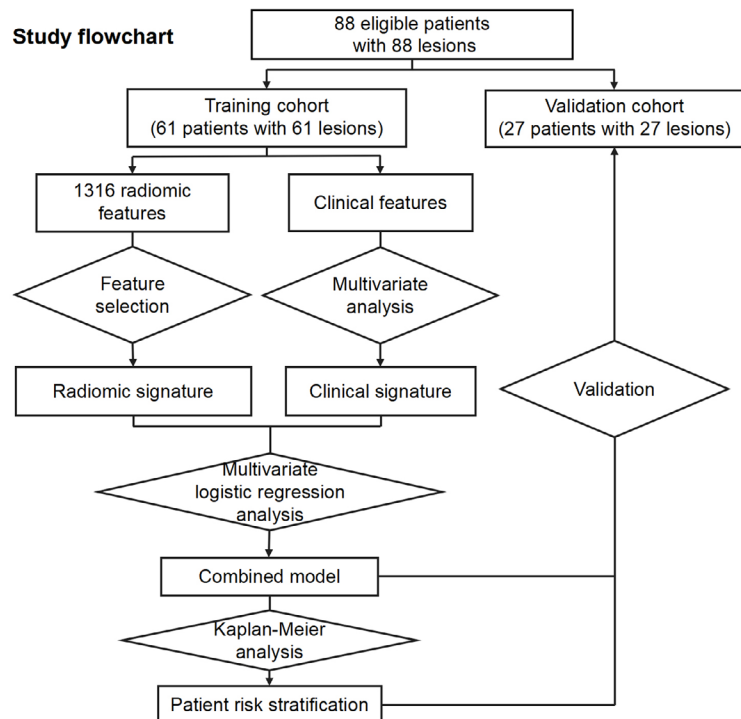


FIGURE 1 Quantitative computed tomography radiomic workflow

is desirable to extract features from conventional clinical and imaging data to assist existing methods for risk stratification and efficacy prediction in patients with tumors; however, there has been limited related research in patients with different ALK variants of lung cancer receiving ALK-TKI treatment.

Here, we collected the genomic-alteration and treatment data of patients with ALK-positive crizotinib-refractory NSCLC enrolled in a phase 2 clinical trial investigating the safety and efficacy of ensartinib, a second-generation ALK inhibitor. We aimed to assess the association of ALK variants and secondary alterations with ensartinib response duration in NSCLC as well as explore the potential value of

clinical and imaging features (conventional imaging features and quantitative radiomic characteristics) in predicting PFS.

## METHODS

### Patients

We retrospectively analyzed the data from a phase II multi-center clinical trial (ClinicalTrials.gov identifier: NCT03215693) between September 2017 and July 2019.<sup>9</sup> The trial was approved by respective local institutional

**TABLE 1** Baseline characteristics of patients ( $n = 88$ ) and lesions ( $n = 88$ ) according to progression-free survival

Variable	Nonprogression group ( $n = 33$ )	Progression group ( $n = 55$ )	<i>p</i> -value
Age (year)	51.00 (44.00, 61.30)	51.00 (41.00, 55.80)	0.363
Sex, male	23 (69.70)	27 (49.09)	0.059
Smoker	12 (36.36)	17 (30.91)	0.598
ECOG, 0/1/2	4/28/1 (12.12/84.85/3.03)	12/42/1 (21.82/76.36/1.82)	0.5
Clinical stage, IIIb/IV	0/33 (0.00/100.00)	1/54 (1.82/98.18)	1.0
Adenocarcinoma/squamous-cell carcinoma/ adenosquamous carcinoma	31/1/1 (93.94/3.03/3.03)	53/2/0 (96.36/3.64/0.00)	0.722
Previous chemotherapy	18 (54.55)	32 (58.18)	0.739
Previous brain radiotherapy <sup>a</sup>	13 (48.15)	12 (31.58)	0.176
Additional therapies between crizotinib and ensartinib <sup>b</sup>	8 (24.24)	5 (9.09)	0.103
Response duration of crizotinib (days)	452.00 (386.00, 743.50)	284.00 (210.40, 366.80)	<0.001
Response duration to crizotinib $\geq 1$ year	28 (84.85)	16 (29.09)	<0.001
Response to crizotinib in early treatment, PR/SD/PD	30/3/0 (90.91/9.09/0.00)	38/16/1 (69.09/29.09/1.82)	0.058
Surgery for primary lung cancer	3 (9.09)	2 (3.64)	0.552
No. of metastatic organs $\geq 3$	19 (57.58)	35 (63.64)	0.572
No. of metastatic tumors $\geq 5$	27 (81.82)	43 (78.18)	0.682
Intrapulmonary metastasis	14 (42.42)	25 (45.45)	0.782
Brain metastasis	27 (81.82)	38 (69.09)	0.188
Lymph node metastasis	18 (54.55)	34 (61.82)	0.502
Pleural metastasis	7 (21.21)	9 (16.36)	0.568
Osseous metastasis	10 (30.30)	29 (52.73)	0.04
Adrenal metastasis	1 (3.03)	3 (5.45)	1.0
Liver metastasis	3 (9.09)	17 (30.91)	0.018
Other metastasis <sup>c</sup>	2 (6.06)	2 (3.64)	1.0
ALK variant, v1/v3/others	7/11/15 (21.21/33.33/45.45)	24/19/12 (43.64/34.55/21.82)	0.035
Secondary ALK alteration	9 (27.27)	31 (56.36)	0.008
Characteristics of the eligible largest target lesions			
Longest-axis diameter (cm)	2.64 (2.04, 4.09)	3.66 (2.13, 4.68)	0.172
Short-axis diameter (cm)	1.37 (0.98, 2.20)	1.64 (1.16, 2.40)	0.291
Volume (cm <sup>3</sup> )	3.47 (1.69, 15.52)	7.95 (1.80, 19.80)	0.169

Note: Data are numbers of patients with percentages in parentheses or medians; interquartile ranges are in parentheses.

Abbreviations: ECOG, Eastern Cooperative Oncology Group performance status; PD, progressive disease; PR, partial response; SD, stable disease.

<sup>a</sup>Among patients with brain metastases at baseline,  $n = 65$ .

<sup>b</sup>Including seven patients who received chemotherapy and one who received radiotherapy in the nonprogression group, and three who received chemotherapy and two who received chemotherapy and EGFR-TKI therapy in the progression group.

<sup>c</sup>Including one with peritoneal metastases in the nonprogression group, and one with renal metastases and one with splenic metastases in the progression group.

review boards. Before trial participation, each patient provided written informed consent.

One hundred and sixty patients with locally advanced or metastatic (stage IIIB/IV) ALK-positive NSCLC from 27 centers across China were enrolled in the clinical trial. We selected eligible patients for this study among the original patient population. The inclusion criteria were: (i) available information on ALK fusion variants; (ii) available information on secondary ALK alterations at baseline; (iii) baseline contrast-enhanced computed tomography (CT) performed within four weeks before ensartinib treatment commencement, with the CT images qualified; and (iv) measurable and describable tumor lesions detected.

Tumor assessments were performed at baseline, every six weeks for the first 24 weeks, and then every nine weeks until disease progression; CT was used to scan the chest, abdomen, and pelvis, and magnetic resonance imaging was used to scan the brain. Diseases were assessed by an independent review committee (IRC) according to Response Evaluation Criteria in Solid Tumors (RECIST) 1.1. Patients were followed up for at least 42 weeks and divided into progression and non-progression groups based on the IRC evaluation results. Each patient's clinical characteristics were obtained by reviewing their medical records.

## ALK fusion and secondary ALK alteration analysis

ALK fusion was confirmed using Ventana immunohistochemistry (Ventana Medical Systems), fluorescence in-situ hybridization, or reverse transcription polymerase chain reaction, either locally or at the central laboratory (Q2 Solutions). The genomic profile of the ALK fusions was investigated using ctDNA assays. Cell-free DNA extraction was performed using the Qiagen QIAamp Circulating Nucleic Acid Kit (Hilden). DNA was analyzed with a 212-gene sequencing panel (Repugene), with mean

sequencing depths of approximately 20 000 times. These analyses were performed at the Repugene Technology Laboratory (Hangzhou, China). The detection methods and gene profiles of the sequencing panel have been described in detail in previously published studies.<sup>9,19</sup>

## CT examination and analysis of CT characteristics

All patients underwent enhanced multidetector row CT from the supraclavicular fossa to the symphysis pubis at baseline. CT images were acquired according to standardized scanning protocols adapted to each center's equipment. The CT parameters were: thickness, 5 mm; spacing interval, 1–5 mm; reconstruction thickness, 0.625–2 mm; reconstruction spacing, 0.5–2 mm; rotation time, 0.28–0.75 s; tube voltage, 100/120 kV; tube current, 50–700 mAs.

Two radiologists (DHH and SJZ, with five and 20 years of experience, respectively, in a full-service academic cancer hospital) reviewed the CT images, selected the eligible largest target lesion of each patient defined by the IRC, recorded its location, and measured its longest and short-axis diameters in the same section at baseline.

Quantitative CT radiomics analysis was performed on the largest target lesions of each patient at baseline. The radiomic workflow is presented in Figure 1. All images were resampled to a voxel size of  $1 \times 1 \times 1 \text{ mm}^3$  using the Artificial Intelligence Kit (AK software; GE Healthcare). Tumor regions of interest were semi-automatically segmented on processed axial enhanced CT images using ITK-SNAP 3.6 (<http://www.itksnap.org>) by a junior radiologist (DHH), and then validated by a senior radiologist (SJZ).

In total, 1316 radiomic features were extracted for each lesion from the CT images using AK software, based on the open-source Pyradiomics Python package, including 18 first-order histograms, 24 gray-level co-occurrence matrices, 14 shapes, 14 gray-level dependence matrices, 16 gray-level size-zone matrices, 16 gray-level run-length matrices,

**TABLE 2** Univariate and multivariate analyses for clinicopathological characteristics between the progression and nonprogression groups

	Nonprogression group ( <i>n</i> = 33)	Progression group ( <i>n</i> = 55)	Univariate analysis	Multivariate analysis		
			<i>p</i> value	Odds ratio	95% CI	<i>p</i> -value
Response duration of crizotinib (days)	452.00 (386.00, 743.50)	284.00 (210.40, 366.80)	<0.001			
Response duration to crizotinib $\geq 1$ year	28 (84.85)	16 (29.09)	<0.001	0.11	0.03, 0.43	0.002
Osseous metastasis	10 (30.30)	29 (52.73)	0.04			
Liver metastasis	3 (9.09)	17 (30.91)	0.018			
ALK variant, v1/v3/others	7/11/15 (21.21/33.33/45.45)	24/19/12 (43.64/34.55/21.82)	0.035			
Secondary ALK alteration	9 (27.27)	31 (56.36)	0.008	5.33	1.48, 19.24	0.011

Note: Data are numbers of patients with percentages in parentheses or medians; interquartile ranges are in parentheses. Abbreviation: CI, confidence interval.

744 wavelets, five neighboring gray-tone difference matrices, 186 Gaussian (LoGsigma = 2.0/3.0), and 279 local binary pattern features. We used three feature selection methods. General univariate and correlation analyses

(threshold, 0.7), to select highly predictive but uncorrelated features, and the least absolute shrinkage and selection operator method were used to select the optimized subset of features and evaluate their corresponding coefficients.<sup>20</sup>

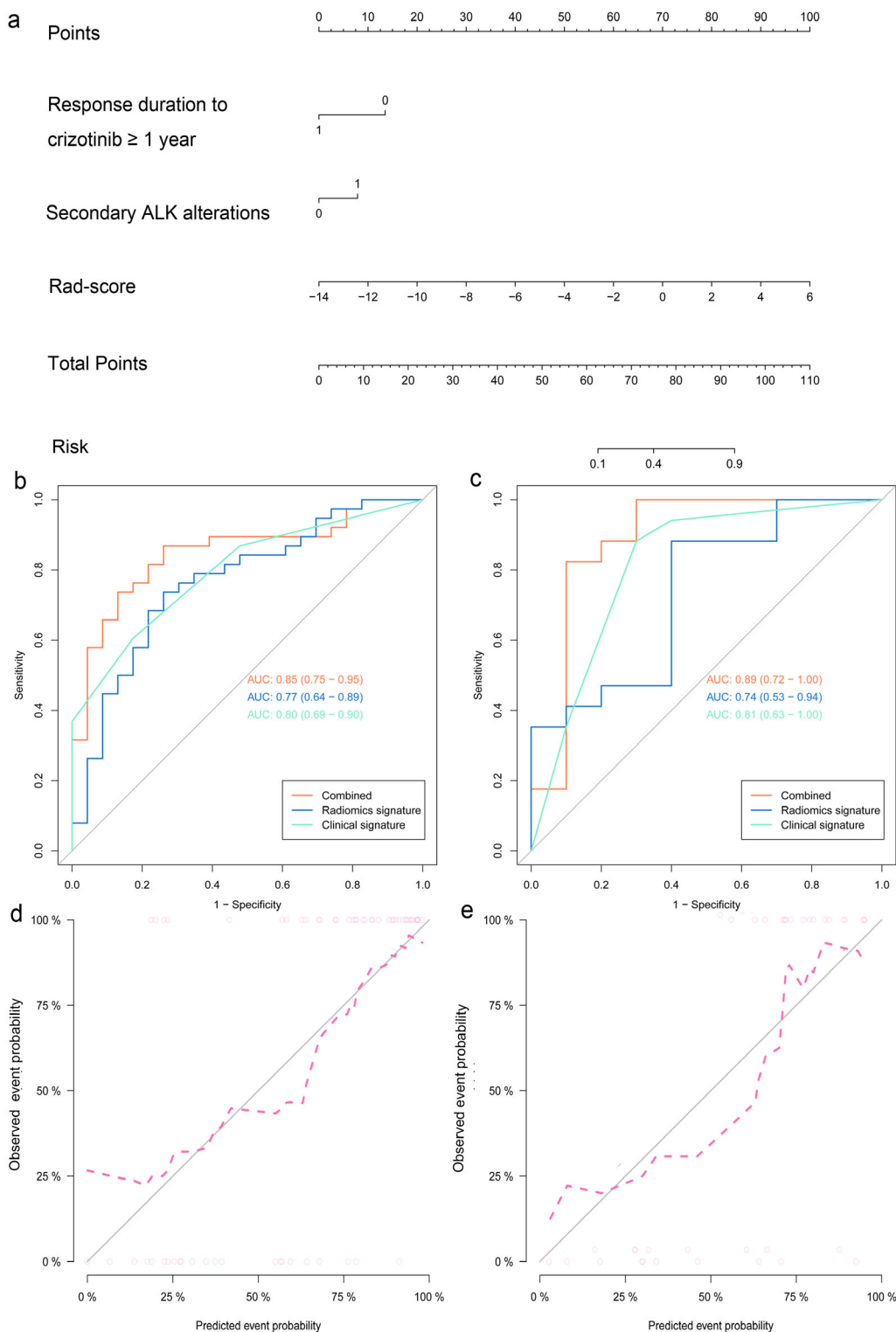


**FIGURE 2** Predictive performance of the clinical signature, radiomic signature, and combined model for predicting progression within 42 weeks. (a) Receiver operating characteristic (ROC) curves for the radiomic signature, clinical signature, and baseline combined model in the training (b) and validation (c) cohorts. Calibration curves of the combined model in the training (d) and validation cohorts (e). AUC: area under the receiver operating characteristic curve

## Statistical analysis

Continuous data that fitted the normal distribution are expressed as mean  $\pm$  standard deviation, while continuous data that did not fit the normal distribution are expressed as the median (range). Categorical data are presented as numbers (percentages). Univariate analyses were performed to assess the differences in clinicopathological and CT imaging characteristics between patients in the progression and non-progression groups. The Mann–Whitney U test was used for continuous variables, and Pearson's chi-square test or Fisher's exact test were used for categorical variables. Multivariate logistic analysis was used to determine independent factors that could discriminate patients in the progression and nonprogression groups; odds ratios (ORs) were also

calculated. Significant ( $p < 0.05$ ) variables in the univariate analyses were included in the multivariate analysis following the stepwise selection method.

The quantitative CT radiomic signature or rad-score was calculated by linearly fitting selected radiomic features after weighting them according to their respective coefficients using logistic regression; comparisons were performed using Wilcoxon's rank-sum test.

To determine the additional value of the quantitative CT radiomic signature, compared to clinicopathological and conventional CT imaging features, we developed and compared three multifactorial models, namely, a clinical signature (identified via the multivariate logistic regression of clinicopathological features and lesion size measured on CT), radiomic signature, and combined model. Patients were randomly

**TABLE 3** Baseline characteristics of patients ( $n = 88$ ) and lesions ( $n = 88$ ) according to ALK variants

Variable	Variant 1 ( $n = 31$ )	Variant 3 ( $n = 30$ )	Other variants ( $n = 27$ )	<i>p</i> -value
Age (year)	47.00 (41.00, 57.80)	53.50 (49.85, 62.00)	46.00 (41.00, 54.00)	0.074
Men	20 (64.52)	13 (43.33)	17 (62.96)	0.184
Smoker	11 (35.48)	8 (26.67)	10 (37.04)	0.660
ECOG score, 0/1/2	5/26/0 (16.13/83.37/0.00)	5/24/1 (16.67 /80.00/3.33)	6/20/1 (22.22 74.07/3.70)	0.805
Clinical stage, IIIb/ IV	1/30 (3.23/96.77)	0/30 (0.00/100.00)	0/27 (0.00100.00)	0.395
Adenocarcinoma/squamous-cell carcinoma/adenosquamous carcinoma	28/2/1 (90.32/6.45/3.23)	30/0/0 (100.00/0.00/0.00)	26/1/0 (96.30/3.70/0.00)	0.425
Additional therapies between crizotinib and ensartinib <sup>a</sup>	3 (9.68)	3 (10.00)	7 (25.93)	0.167
Response duration to crizotinib (days)	308.00 (221.60, 455.00)	366.00 (227.90, 498.10)	389.00 (231.20, 661.20)	0.446
Response duration to crizotinib $\geq 1$ year	11 (35.48)	16 (53.33)	17 (62.96)	0.102
Response to crizotinib in early treatment, PR/SD/PD	22/9/0 (70.97/29.03/0.00)	25/4/1 (83.33/13.33/3.33)	21/6/0 (77.78/22.22/70.00)	0.408
Response to ensartinib in early treatment, PR/SD/PD	16/12/3 (51.61/38.71/9.68)	15/14/1 (50.00/46.67/3.33)	13 (48.15/44.44/7.41)	0.899
Surgery for primary lung cancer	1 (3.23)	4 (13.33)	0 (0.00)	0.100
No. of metastatic organs $\geq 3$	19 (61.29)	18 (60.00)	17 (62.96)	0.974
No. of metastatic tumors $\geq 5$	24 (77.42)	24 (80.00)	22 (81.48)	0.927
Intrapulmonary metastasis	12 (38.71)	16 (53.33)	11 (40.74)	0.467
Brain metastasis	24 (77.42)	20 (66.67)	21 (77.78)	0.543
Lymph node metastasis	18 (58.06)	21 (70.00)	13 (48.15)	0.243
Pleural metastasis	7 (22.58)	6 (20.00)	3 (11.11)	0.502
Osseous metastasis	16 (51.61)	9 (30.00)	14 (51.85)	0.151
Adrenal metastasis	1 (3.23)	3 (10.00)	0 (0.00)	0.262
Liver metastasis	5 (16.13)	7 (23.33)	8 (29.63)	0.471
Other metastases <sup>b</sup>	1 (3.23)	2 (6.67)	0 (0.00)	0.644
Secondary ALK alteration	13 (41.94)	18 (60.00)	9 (33.33)	0.116
Characteristics of the eligible largest target lesions				
longest-axis diameter (cm)	3.00 (1.84, 4.49)	2.90 (2.26, 4.35)	3.56 (2.44, 4.86)	0.474
Short-axis diameter (cm)	1.51 (1.03, 2.20)	1.65 (0.84, 2.16)	1.64 (1.10, 2.40)	0.731
Volume (cm <sup>3</sup> )	5.40 (1.69, 15.31)	5.68 (1.23, 19.56)	8.79 (2.08, 18.24)	0.627

<sup>a</sup>Including two patients who received chemotherapy, and one who received chemotherapy and EGFR-TKI therapy in the V1 group; three who received chemotherapy, one who received radiotherapy, and one who received EGFR-TKI therapy in the V3 group; five patients who received chemotherapy, and one who received chemotherapy and EGFR-TKI therapy in the other ALK variant group.

<sup>b</sup>Including one with splenic metastases in the V1 group, and one each with renal metastases and peritoneal metastases in the V3 group.

Abbreviations: ECOG, Eastern Cooperative Oncology Group performance status; PD, progressive disease; PR, partial response; SD, stable disease.

divided into training and validation datasets at a 7:3 ratio. The area under the receiver operating characteristic curve (AUC), accuracy, sensitivity, and specificity were used to evaluate the performance of the three models in the validation dataset. The calibration curve and Hosmer-Lemeshow test were used to assess the calibration and goodness-of-fit of the combined model.<sup>21</sup> Decision curve analysis was conducted to independently evaluate the clinical value of the three models based on the calculation of the net benefit for patients at each threshold probability. By comparing to all or no strategies, the best model was selected according to the highest calculated net benefit. The relationship between the radiomic signature, clinicopathological features, and combined model and PFS was further assessed using Kaplan–Meier analysis. The thresholds of the rad-score and combined model, used to group high and

low risks, were calculated using logistic regression. The differences in survival curves were evaluated using the log-rank test.

All statistical analyses in the present study were performed using R (<https://mran.microsoft.com>; version 3.5.1) and Python (<https://www.python.org>; version 3.5.6). Statistical significance was defined as a two-tailed  $p$ -value  $< 0.05$ .

## RESULTS

### Patients and clinicopathological characteristics

Baseline patient characteristics are listed in Table 1. Eighty-eight eligible patients with clarified ALK variants were included in this study; median age was 51 years (range, 23–

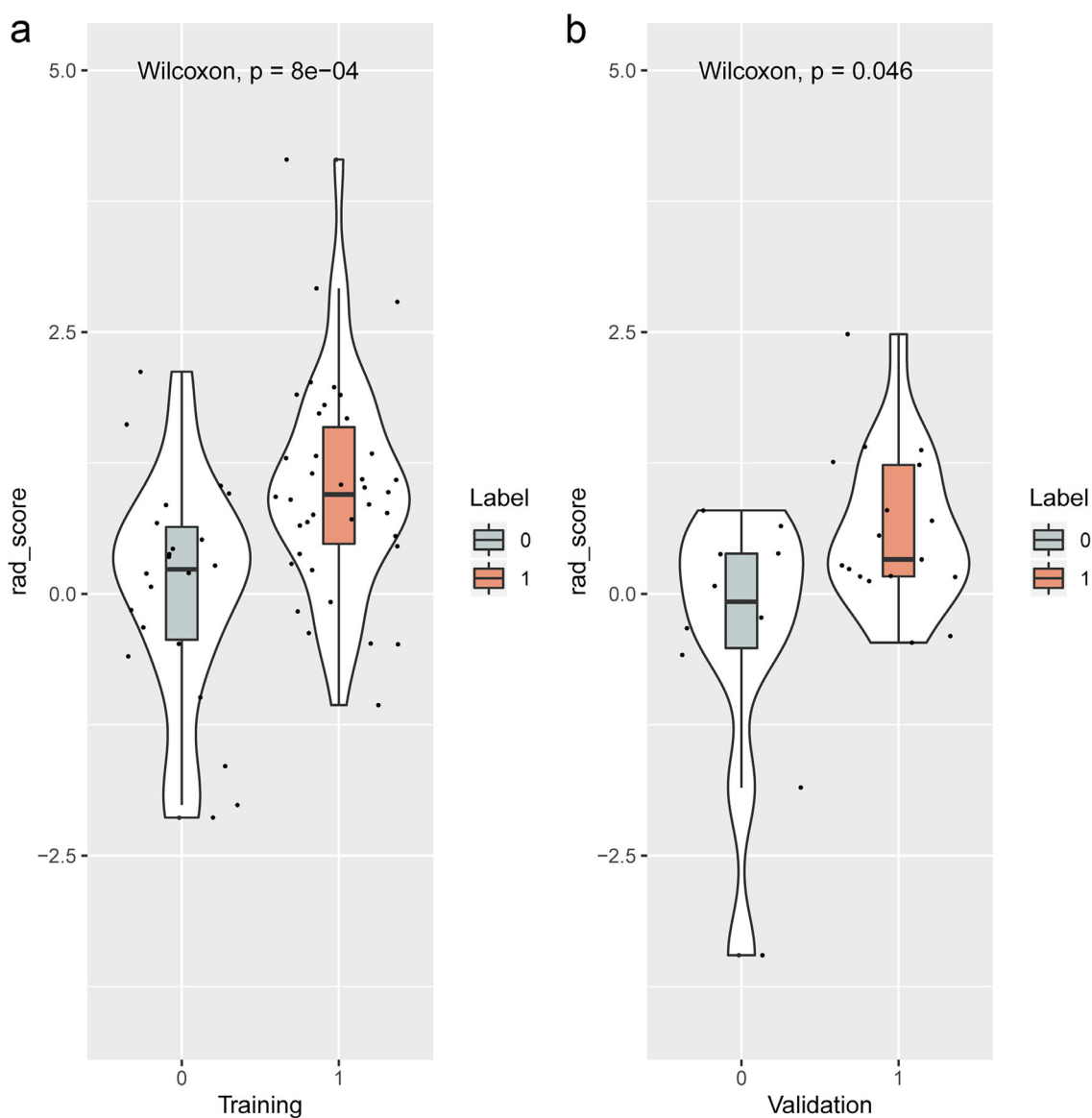


**FIGURE 3** Box plots of the rad-scores. The box plots (a) and (b) show the difference in the rad-score between the progression and nonprogression groups in the training (a) and validation (b) cohorts, respectively. The  $p$ -values were obtained using the Wilcoxon rank-sum test. Label 0, shown in sage green, represents the nonprogression group; Label 1, shown in orange, represents the progression group

69 years), and 50 patients (57%) were men. Among them, 78 (89%) had an EML4-ALK fusion. The most frequent EML4-ALK variants were v1, in 31 patients, (40%) and v3, in 30 patients (38%). Remaining EML4-ALK fusions consisted of v2 (12, 15%, [E20;A20]), v5' (3, 4%, [E18;A20]), and v5a (2, 3%, [E2;A20]). Among the non-EML4-ALK fusions detected in 10 patients (11%), the fusion partner genes included *HIP1* ( $n = 2$ ), *DCHS1* ( $n = 1$ ), *INHBA* ( $n = 1$ ), *PPFIBP1* ( $n = 1$ ), *KIF5B* ( $n = 1$ ), *PSMC4* ( $n = 1$ ), *SEC31A* ( $n = 1$ ), *TIMP3* ( $n = 1$ ), and *ZNF69* ( $n = 1$ ). At baseline, 40 (31%) patients had secondary ALK alterations (point mutations or copy number variation), while three (3%) patients had genetic alterations that could have mediated bypass signaling (PIK3CA, erb-B2, KRAS).

Among the 88 patients, 55 were in progression group and 33 were in non-progression group. In the univariate analyses, patients in the progression group tended to have shorter response duration to crizotinib ( $p < 0.001$ ), more frequent osseous metastasis ( $p = 0.04$ ) and liver metastasis ( $p = 0.018$ ), and more commonly occurring secondary ALK alterations ( $P = 0.008$ ), than those in the non-progression group. The distribution of ALK variants also differed between the two groups; V2/5/5a/non-EML4 ALK variants were more common in the non-progression group, whereas V1 was more common in the progression group ( $p = 0.035$ ). In the multivariate logistic regression of conventional clinicopathological characteristics, response duration to crizotinib  $\geq 1$  year (OR, 0.14; 95% confidence interval [CI]: 0.04, 0.48;  $p = 0.002$ ), and secondary ALK alterations (OR, 3.92; 95% CI, 1.30, 11.84;  $p = 0.016$ ) remained significant for discriminating patients to either the progression or nonprogression group (Table 2). The clinical signature, composed of the

remaining features, attained an AUC, accuracy, sensitivity, and specificity of 0.80 (95% CI: 0.69 to 0.90), 68.9%, 85.2%, and 55.9%, respectively, in the training dataset and 0.81 (95% CI: 0.63 to 1.00), 81.5%, 83.3%, and 77.8%, respectively, in the validation dataset (Figure 2(b),(c); Supplementary Table S1).

The clinical characteristics according to ALK variant are summarized in Table 3. Secondary ALK alterations were more common in patients with the V3 variant (60.00%) than with the V1 (41.94%) and other (33.33%) variants, although this difference was not statistically significant ( $p = 0.116$ ; Figure S1(a)). A detailed list of secondary ALK alterations is provided in Table S2 and Figure S1(b). L1196M (five, three, and two patients with V1, V3, and other variants, respectively), C1156Y (five patients with V3, one patient with V1), F1174L (five patients with V3, one patient with the [TIMP3\_E1;ALK\_E20] variant), and G1202R (four patients with V3, one patient with V5a, one patient with the [ZNF69\_E4;ALK\_E20] variant) were the most commonly occurring point mutations. There was no significant difference in the response and response duration to crizotinib according to the ALK fusion variant. Other clinicopathological parameters did not differ according to the ALK variant.

### Analysis of quantitative CT radiomic features

A total of 1316 delta radiomic features were extracted for each lesion. Eight features with nonzero coefficients were selected. The rad-score calculation formula is presented in Supplementary Material S1.

Rad-scores were significantly higher in the progression group than in the nonprogression group, both in the

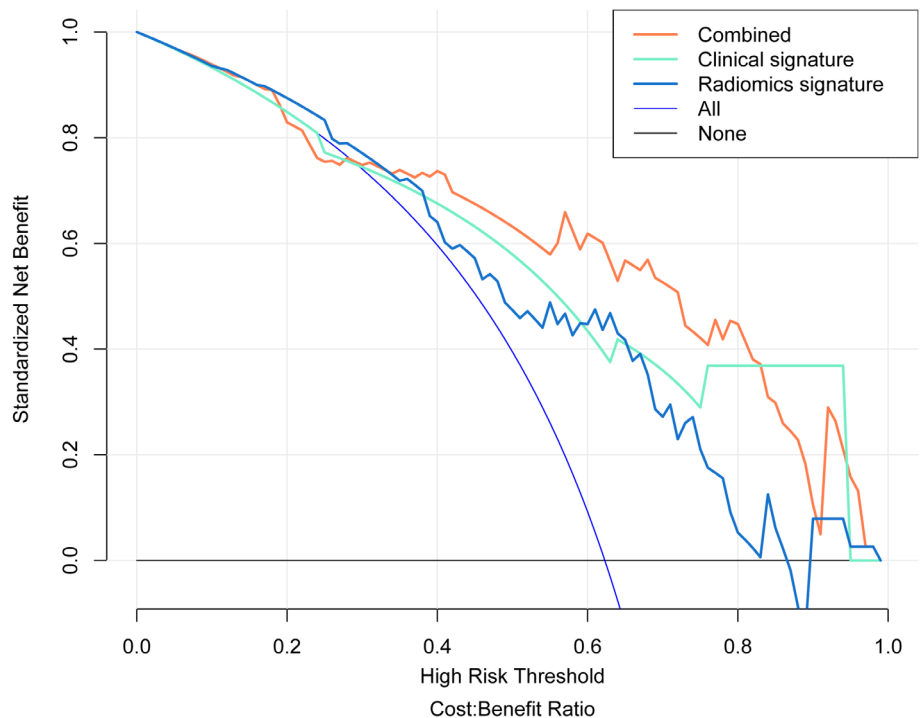


**FIGURE 4** Decision curve analysis for the combined model. The y-axis represents the net benefit. The light purple line represents the hypothesis that all patients progressed within 42 weeks; the black line represents the hypothesis that no patient progressed within 42 weeks. Compared to the CT radiomic or clinical signatures alone, the combined model (orange in the figure) improved the performance of progress prediction with more areas



training and validation data sets ( $p < 0.001$  and  $p = 0.046$ , respectively; Wilcoxon's rank-sum test; Figure 3(a),(b)).

The radiomic signature achieved an AUC, accuracy, sensitivity, and specificity of 0.77 (95% CI: 0.64 to 0.89), 73.8%, 73.7%, and 73.9%, respectively, in the training dataset and 0.74 (95% CI: 0.53 to 0.94), 59.3%, 47.1%, and 80.0%,

respectively, in the validation data set (Figure 2(b),(c); Table 1).

A combined model was constructed by incorporating the radiomic signature and the remaining statistically significant clinical features (Figure 2(a)). The combined model yielded an AUC, accuracy, sensitivity, and specificity of 0.85 (95% CI: 0.75 to 0.95), 82.0%, 84.6%, and 77.3%,

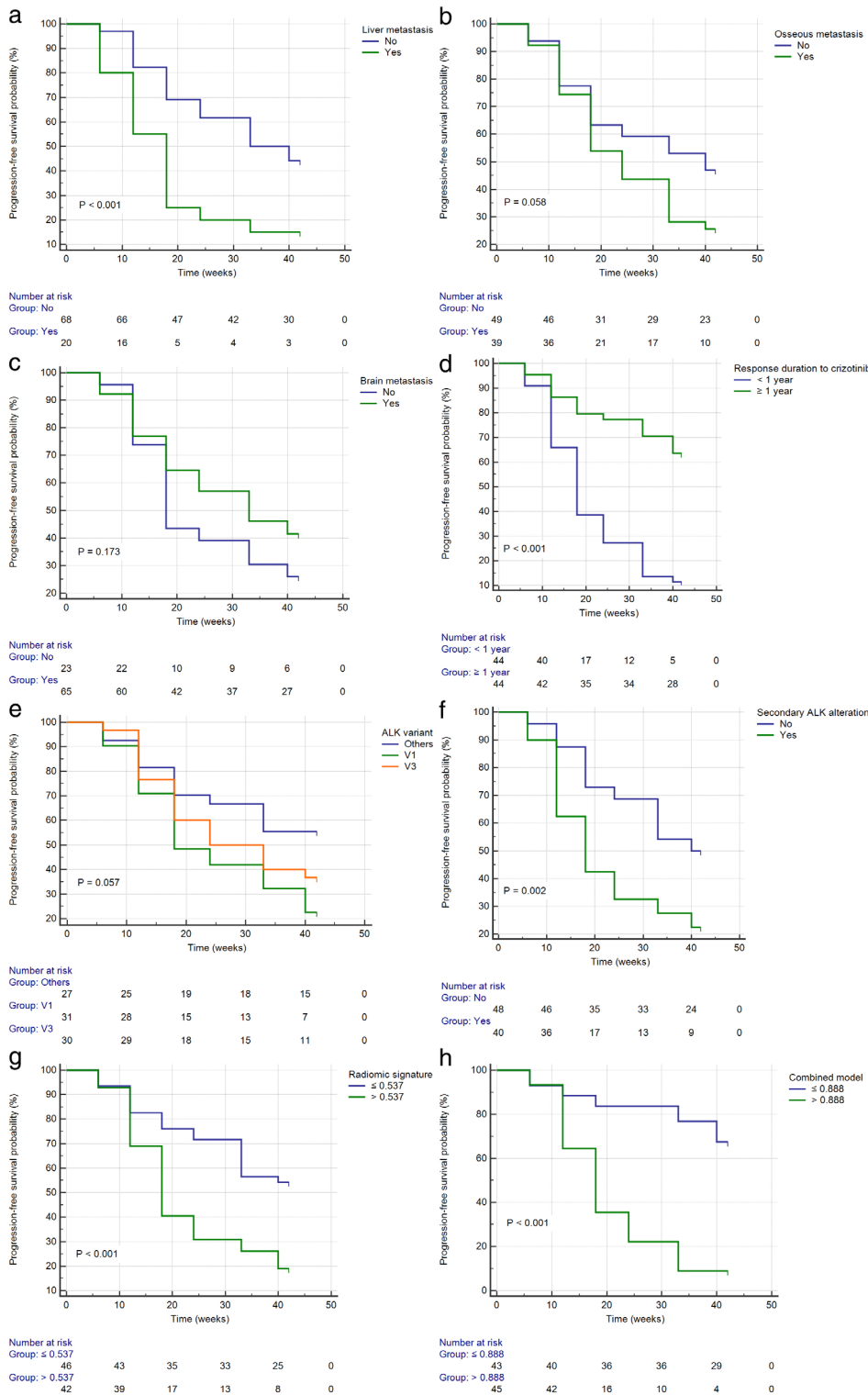


**FIGURE 5** Kaplan–Meier plot for time to progression based on the combined models, radiomic signatures, and clinical features. (a), liver metastasis; (b), osseous metastasis; (c), brain metastasis; (d), response duration to crizotinib; (e), ALK variant; (f), secondary ALK alteration; (g), radiomic signature; (h), combined model

respectively, in the training dataset and 0.89 (95% CI: 0.72 to 1.00), 85.2%, 93.3%, and 75.0%, respectively, in the validation dataset (Figure 2(b),(c); Table 1), indicating that the radiomic signature provided added value to the conventional clinicopathological features in terms of discriminatory efficacy. The calibration curve of the combined model is shown in Figure 2(d),(e). The Hosmer-Lemeshow test yielded  $p$ -values of 0.761 and 0.680 in the training and validation datasets, respectively, indicating good calibration power. According to the decision curve, the combined model achieved improved tumor progression prediction, with more areas shown in the validation cohort compared to the model derived from the radiomic signature or the clinical signature alone (Figure 4, decision curve analysis). Simply put, although CT radiomic features alone have inferior predictive performance than the clinical model, combination of the two can increase the predictive performance of the clinical model.

### Patient risk stratification

Kaplan–Meier analysis, defined by radiomic signatures, the selected clinicopathological features, and the combined model showed that liver metastasis (log-rank,  $p < 0.001$ ), response duration to crizotinib  $\geq 1$  year (log-rank,  $p < 0.001$ ), secondary ALK alteration (log-rank,  $p = 0.002$ ), radiomic signature  $>0.537$  (log-rank,  $p < 0.001$ ), and combined model  $>0.888$  (log-rank,  $p < 0.001$ ) could distinguish patients with higher risk of tumor progression within 42 weeks, whereas other clinical features displayed no significant survival difference (Figure 5).

### DISCUSSION

In this study, we examined the effects of ALK variants and ALK resistance mutations on the clinical outcomes of ALK-positive NSCLC patients treated with ensartinib, and evaluated the prognostic value of clinical and CT imaging features. A significant strength of the study was that we used prospectively acquired high-quality data from a clinical trial, which had predefined criteria for patient enrollment, treatment, and follow-up.

As described in the Introduction, previous studies have reported clinical responses to ALK-TKIs according to the ALK variant, with conflicting results found for the same and different TKIs.<sup>13–18</sup> In our study, although ALK variants in three classifications (V1, V3, other variants) were correlated with the PFS of patients treated with ensartinib in the univariate analysis, in the multivariate and Kaplan–Meier analyses, this association was not statistically significant. In addition, no significant differences were found in the response and response duration to crizotinib and other clinicopathological characteristics according to the ALK fusion variant (Table 3). Further, there were no statistically significant differences between the most common variants, V1 and

V3, in terms of both clinicopathological characteristics and response and response duration to crizotinib/ensartinib (Table 3). Therefore, the ALK variant may have little effect on the efficacy of ensartinib.

Consistent with the results of previous studies,<sup>22–26</sup> secondary ALK alterations were adversely associated with PFS, both in the univariate and multivariate analyses, and could identify patients at high risk for early progression in the Kaplan–Meier analysis. As in previous studies,<sup>16,22</sup> secondary ALK mutations were more common in V3; however, they were not statistically significant in this study because of the small number of patients. Interestingly, patients with V3, which has a greater propensity to develop ALK mutations, tended to have longer PFS than patients with V1 (Figure 5(e),  $p = 0.057$ ), contrary to previous findings.<sup>13–15</sup> We speculate that the different distribution of secondary point mutations between V1 and V3, and the different activities of ensartinib against various ALK resistance mutations, likely underlie this outcome. Supportive of this notion, ensartinib is active against a broad array of ALK mutations, including C1156Y, F1174, G1269A, I1171, L1152R/V, and even G1202R, which are more common in V3, but has low activity in patients with the L1196M mutation (the proportion with an objective response was only 25%), which is more common in V1.<sup>9</sup>

In view of the above results, we speculate that the conflicting results of previous studies on the effect of ALK subtypes on the efficacy of TKIs may be attributed to the small sample size and inconsistent clustering of variants into groups. Moreover, secondary ALK mutations differing among ALK variants and the unique spectrum of activity of each ALK inhibitor against different ALK resistance mutations may also play a role. In other words, differences in the efficacy of TKIs among ALK variants might stem from differences in the secondary ALK mutations among them; when the spectrum of activity of TKIs against secondary ALK mutations changed, the difference in efficacy among ALK variants would also change. Notably, secondary mutations are more common in V3, which may be the reason it is associated with poor efficacy in most studies.

In addition to ALK variants and secondary ALK mutations, the response duration to crizotinib, liver metastases, and bone metastases also had predictive significance for the progression of patients during the median PFS (42 weeks). The shorter effective response duration to crizotinib was also a risk factor for early progression in patients treated with ensartinib, and similar performance has been observed in clinical studies of other ALK-targeted inhibitors.<sup>12,27,28</sup> Liver and osseous metastases are known factors for poor prognosis in certain cancers and various treatments.<sup>29–31</sup> Notably, brain metastasis is also a factor leading to poor prognosis or progression of ALK-positive NSCLC.<sup>32,33</sup> However, in our study, brain metastasis was not a statistically significant factor for progression within 42 weeks, and there was no significant difference in the survival curve of patients with brain metastasis in the Kaplan–Meier analysis, which may be related to the excellent efficacy of ensartinib in the central nervous system.<sup>9,34</sup>

Combined with the quantitative CT radiomic signature, the predictive performance of conventional clinicopathological features for PFS could be increased. When patients cannot tolerate biopsy or the biopsy/ctDNA test is negative, but other clinical indications suggest that the patients may be at high risk, quantitative radiomics may assist in the clinical identification of patients at high risk to appropriately increase the frequency of follow-up and adjust the treatment in a timely manner. Although radiomics, as the product of medical and engineering cross-development, has emerged in the diagnosis and efficacy evaluation of tumors, there remains room for improvement and standardization.<sup>35,36</sup>

The current study had several limitations. First, as this was a retrospective study with a small sample size, we clustered all rare ALK fusion variants (V2/V5<sup>\*</sup>/V5a/non-EML4 variants) into one general subgroup; the biological and clinical features among them may not be relevant. Second, as the tumor tissue of some patients could not be obtained, the analysis of ALK variants and ALK secondary mutations were based on ctDNA-NGS test, which has several drawbacks,<sup>37</sup> such as the detection of hotspot mutations only in the coding regions of prespecified genes by the NGS panel, underestimation of alterations in other genomic regions, and the inadequate sensitivity of the ctDNA-based NGS may result in false-negative, especially for gene rearrangement. Third, the number of patients in the progression and nonprogression groups was imbalanced (55 VS 33), which could be related to the efficiency of ALK mutation recognition in the blood and may have caused statistical analysis bias, affecting the predictive capability and accuracy of the model. Thus, the results should be interpreted with caution and further verified using different detection methods (such as PCR) and tissue biopsy in a large cohort.

In summary, our study showed that secondary ALK alterations were adversely associated with ensartinib efficacy and that ALK variants might not be correlated with PFS. We speculate that the secondary ALK mutations differing among ALK variants and the unique spectrum of activity of each ALK inhibitor against different ALK resistance mutations were responsible for the different efficacy of TKIs in different ALK variants in previous studies. Moreover, we found that quantitative radiomics may assist in the clinical identification of patients at high risk for early progression, which requires confirmation via further studies with larger cohorts.

## ACKNOWLEDGMENTS

This work was supported by the National Key R&D Program of China (No. 2017YFC1308700), CAMS Innovation Fund for Medical Sciences (No. 2017-I2M-1-005, 2019-I2M-2-002), the National Natural Science Foundation of China (No. 81771830), and the Beijing Municipal Science and Technology Project (No. Z201100005620002).

## CONFLICT OF INTEREST

Lieming Ding is an employee of Betta Pharmaceuticals. The other authors declare no potential conflicts of interest.

## ORCID

Donghui Hou  <https://orcid.org/0000-0001-8749-4741>

Shijun Zhao  <https://orcid.org/0000-0001-5554-0336>

## REFERENCES

- Katayama R, Lovly CM, Shaw AT. Therapeutic targeting of anaplastic lymphoma kinase in lung cancer: a paradigm for precision cancer medicine. *Clin Cancer Res*. 2015;21:2227–35.
- Sabir SR, Yeoh S, Jackson G, Bayliss R. EML4-ALK variants: biological and molecular properties, and the implications for patients. *Cancers (Basel)*. 2017;9:E118.
- Hong M, Kim RN, Song JY, Choi SJ, Oh E, Lira ME, et al. HIP1-ALK, a novel fusion protein identified in lung adenocarcinoma. *J Thorac Oncol*. 2014;9:419–22.
- Togashi Y, Soda M, Sakata S, Sugawara E, Hatano S, Asaka R, et al. KLC1-ALK: a novel fusion in lung cancer identified using a formalin-fixed paraffin-embedded tissue only. *PLoS One*. 2012;7:e31323.
- Takeuchi K, Choi YL, Togashi Y, Soda M, Hatano S, Inamura K, et al. KIF5B-ALK, a novel fusion onco kinase identified by an immunohistochemistry-based diagnostic system for ALK-positive lung cancer. *Clin Cancer Res*. 2009;15:3143–9.
- Choi YL, Lira ME, Hong M, Kim RN, Choi SJ, Song JY, et al. A novel fusion of TPR and ALK in lung adenocarcinoma. *J Thorac Oncol*. 2014;9:563–6.
- Masood A, Christ T, Asif S, Rajakumar P, Gustafson BA, Shune LO, et al. Non-secretory multiple myeloma with unusual TFG-ALK fusion showed dramatic response to ALK inhibition. *NPJ Genom Med*. 2021; 6:23.
- Shaw AT, Kim DW, Nakagawa K, Seto T, Crinó L, Ahn MJ, et al. Crizotinib versus chemotherapy in advanced ALK-positive lung cancer. *N Engl J Med*. 2013;368:2385–94.
- Yang Y, Zhou J, Zhou J, Feng J, Zhuang W, Chen J, et al. Efficacy, safety, and biomarker analysis of ensartinib in crizotinib-resistant, ALK-positive non-small-cell lung cancer: a multicentre, phase 2 trial. *Lancet Respir Med*. 2020;8:45–53.
- Shaw AT, Gandhi L, Gadgeel S, Riely GJ, Cetnar J, West H, et al. Alectinib in ALK-positive, crizotinib-resistant, non-small-cell lung cancer: a single-group, multicentre, phase 2 trial. *Lancet Oncol*. 2016; 17:234–42.
- Kim DW, Tiseo M, Ahn MJ, Reckamp KL, Hansen KH, Kim SW, et al. Brigatinib in patients with crizotinib-refractory anaplastic lymphoma kinase-positive non-small-cell lung cancer: a randomized, multicenter phase II trial. *J Clin Oncol*. 2017;35:2490–8.
- Shaw AT, Felip E, Bauer TM, Besse B, Navarro A, Postel-Vinay S, et al. Lorlatinib in non-small-cell lung cancer with ALK or ROS1 rearrangement: an international, multicentre, open-label, single-arm first-in-man phase 1 trial. *Lancet Oncol*. 2017;18:1590–9.
- Su Y, Long X, Song Y, Chen P, Li S, Yang H, et al. Distribution of ALK fusion variants and correlation with clinical outcomes in Chinese patients with non-small cell lung cancer treated with crizotinib. *Target Oncol*. 2019;14:159–68.
- McLeer-Florin A, Duruisseau M, Pinsolle J, Dubourd S, Mondet J, Houllbracq MP, et al. ALK fusion variants detection by targeted RNA-next generation sequencing and clinical responses to crizotinib in ALK-positive non-small cell lung cancer. *Lung Cancer*. 2018;116: 15–24.
- Woo CG, Seo S, Kim SW, Jang SJ, Park KS, Song JY, et al. Differential protein stability and clinical responses of EML4-ALK fusion variants to various ALK inhibitors in advanced ALK-rearranged non-small cell lung cancer. *Ann Oncol*. 2017;28:791–7.
- Lin JJ, Zhu VW, Yoda S, Yeap BY, Schrock AB, Dagogo-Jack I, et al. Impact of EML4-ALK variant on resistance mechanisms and clinical outcomes in ALK-positive lung cancer. *J Clin Oncol*. 2018;36:1199–206.
- Lei YY, Yang JJ, Zhang XC, Zhong WZ, Zhou Q, Tu HY, et al. Anaplastic lymphoma kinase variants and the percentage of ALK-positive tumor cells and the efficacy of crizotinib in advanced NSCLC. *Clin Lung Cancer*. 2016;17:223–31.

18. Cha YJ, Kim HR, Shim HS. Clinical outcomes in ALK-rearranged lung adenocarcinomas according to ALK fusion variants. *J Transl Med.* 2016;14:296.
19. Yang Y, Huang J, Wang T, Zhou J, Zheng J, Feng J, et al. Decoding the evolutionary response to ensartinib in patients with ALK-positive NSCLC by dynamic circulating tumor DNA sequencing. *J Thorac Oncol.* 2021;16:827–39.
20. Tibshirani R. Regression shrinkage and selection via the lasso: a retrospective. *J R Stat Soc Ser B.* 2011;73:273–82.
21. Kramer AA, Zimmerman JE. Assessing the calibration of mortality benchmarks in critical care: the Hosmer-Lemeshow test revisited. *Crit Care Med.* 2007;35:2052–6.
22. Mezquita L, Swalduz A, Jovelet C, Ortiz-Cuaran S, Howarth K, Planchard D, et al. Clinical relevance of an amplicon-based liquid biopsy for detecting ALK and ROS1 fusion and resistance mutations in patients with non-small-cell lung cancer. *JCO Precis Oncol.* 2020;4:PO.19.00281.
23. McCoach CE, Le AT, Gowan K, Jones K, Schubert L, Doak A, et al. Resistance mechanisms to targeted therapies in ROS1+ and ALK+ non-small cell lung cancer. *Clin Cancer Res.* 2018;24:3334–7.
24. Noé J, Lovejoy A, Ou SI, Yaung SJ, Bordogna W, Klass DM, et al. ALK mutation status before and after alectinib treatment in locally advanced or metastatic ALK-positive NSCLC: pooled analysis of two prospective trials. *J Thorac Oncol.* 2020;15:601–8.
25. Haratake N, Seto T, Takamori S, Toyozawa R, Nosaki K, Miura N, et al. Short progression-free survival of ALK inhibitors sensitive to secondary mutations in ALK-positive NSCLC patients. *Thorac Cancer.* 2019;10:1779–87.
26. Jamme P, Descarpentries C, Gervais R, Dansin E, Wislez M, Grégoire V, et al. Relevance of detection of mechanisms of resistance to ALK inhibitors in ALK-rearranged NSCLC in routine practice. *Clin Lung Cancer.* 2019;20:297–304.
27. Camidge DR, Kim HR, Ahn MJ, Yang JC, Han JY, Lee JS, et al. Brigatinib versus crizotinib in ALK-positive non-small-cell lung cancer. *N Engl J Med.* 2018;379:2027–39.
28. Kim DW, Mehra R, Tan DSW, Felip E, Chow LQ, Camidge DR, et al. Activity and safety of ceritinib in patients with ALK-rearranged non-small-cell lung cancer (ASCEND-1): updated results from the multicentre, open-label, phase 1 trial. *Lancet Oncol.* 2016;17:452–63.
29. Riihimäki M, Hemminki A, Fallah M, Thomsen H, Sundquist K, Sundquist J, et al. Metastatic sites and survival in lung cancer. *Lung Cancer.* 2014;86:78–84.
30. Wu KL, Tsai MJ, Yang CJ, Chang WA, Hung JY, Yen CJ, et al. Liver metastasis predicts poorer prognosis in stage IV lung adenocarcinoma patients receiving first-line gefitinib. *Lung Cancer.* 2015;88:187–94.
31. Coleman RE. Skeletal complications of malignancy. *Cancer.* 1997;80:1588–94.
32. Gállego Pérez-Larraya J, Hildebrand J. Brain metastases. *Handb Clin Neurol.* 2014;121:1143–57.
33. de Cos Escuín JS, Arca JA, Íñiguez RM, Sorribes LM, Ares AN, Hernández JR, et al. Tumor, node and metastasis classification of lung cancer—M1a versus M1b—analysis of M descriptors and other prognostic factors. *Lung Cancer.* 2014;84:182–9.
34. Zhang I, Zaorsky NG, Palmer JD, Mehra R, Lu B. Targeting brain metastases in ALK-rearranged non-small-cell lung cancer. *Lancet Oncol.* 2015;16:e510–21.
35. Grossmann P, Narayan V, Chang K, Rahman R, Abrey L, Reardon DA, et al. Quantitative imaging biomarkers for risk stratification of patients with recurrent glioblastoma treated with bevacizumab. *Neuro Oncol.* 2017;19:1688–97.
36. Trebeschi S, Drago SG, Birkbak NJ, Kurilova I, Călin AM, Pizzi AD, et al. Predicting response to cancer immunotherapy using noninvasive radiomic biomarkers. *Ann Oncol.* 2019;30:998–1004.
37. Benayed R, Offin M, Mullaney K, Sukhadia P, Rios K, Desmeules P, et al. High yield of RNA sequencing for targetable kinase fusions in lung adenocarcinomas with no mitogenic driver alteration detected by DNA sequencing and low tumor mutation burden. *Clin Cancer Res.* 2019;25:4712–22.

## SUPPORTING INFORMATION

Additional supporting information may be found online in the Supporting Information section at the end of this article.

**How to cite this article:** Hou D, Zheng X, Song W, Liu X, Wang S, Zhou L, et al. Association of anaplastic lymphoma kinase variants and alterations with ensartinib response duration in non-small cell lung cancer. *Thorac Cancer.* 2021;12:2388–99. <https://doi.org/10.1111/1759-7714.14083>